A Numerical Solution for the Near and Far Fields of an Annular Ring of Magnetic Current

LEONARD L. TSAI, MEMBER, IEEE

Abstract—A simple method for calculating the near and far zone fields from an annular ring of circumferentially directed magnetic current which may be used to represent coaxial apertures is presented. Near-field contours are given for two ring sizes. The utility of the method has been illustrated by its application in several practical antenna problems where the magnetic ring current serves as the primary source. Among these are the analysis of dipole antennas mounted on a conducting sphere or cylinder, the impedance of a coaxially fed Yagi–Uda antenna, a coaxially driven wire loop, and the radiation from a coaxial aperture at the base of a cone.

Introduction

In THE determination of impedances for balanced antennas such as a cylindrical dipole, the image-plane method is frequently used. If this ground-plane mounted antenna is driven coaxially, then the distributed source representation of the feed, as originally suggested in [1] and implemented in [2]–[4] for the cylindrical dipole, can be used to better correlate the theoretical and experimental models. The basic idea is that the current in the coaxial feeding aperture is interpreted as the primary source which then excites the rest of the antenna. Accurate results have been obtained [2]–[4] for the cylindrical dipole, and applications of this idea to several other problems appear promising. Hence the fields of the coaxial source are of interest.

There exist in the literature several methods for determining the fields of coaxial sources. The far-zone fields for ring currents are given by [5], [6], and [7] gives the fields for a vanishing small ring. In [8], [9] the coaxial aperture problem is carefully solved by mode matching, but the resultant near-field expressions involve complex infinite integrals of Bessel functions which may be costly to evaluate. In this presentation, a simple numerical scheme is given which readily allows the determination of fields in the near zone, in fact, even inside the ring. Results are also given showing the contour variations of the near fields for some examples.

Manuscript received August 25, 1971; revised March 27, 1972. Portions of this work were presented at the 1970 Spring URSI Meeting, Washington, D. C., April 16–18. This work was supported in part by the Department of the Air Force under a subcontract of M.I.T. Lincoln Laboratory with the Ohio State University Research Foundation and in part by the NSF under Grant NSF/GU 3833 with the University of Mississippi.

The author was with the ElectroScience Laboratory, Department of Electrical Engineering, Ohio State University, Columbus, Ohio 43212. He is now with the Department of Electrical Engineering, University of Mississippi, University, Miss. 38677.

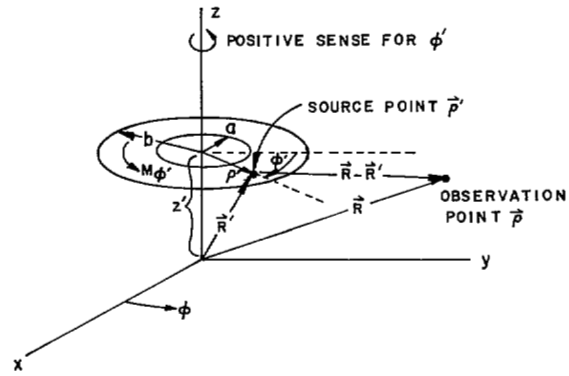

Fig. 1. Geometry of magnetic frill source.

Consider a coaxial aperture terminated in an infinite ground plane. A combination of the equivalence principle and image theory [7] then allows it to be represented simply as an annular ring (or frill) of magnetic current. The geometry of the problem is depicted in Fig. 1, where the annulus has inner and outer coax radii a and b, respectively, and is centrally located along the z axis at $z = z'$. Making the usual TEM mode assumption, the aperture distribution of the coax is

$$E_{\rho'}(\rho') = \frac{1}{2\rho' \ln (b/a)} \quad \text{V/m} \tag{1}$$

for a 1-V excitation. Hence the corresponding magnetic current distribution by image theory is

$$M_{\Phi}' = \frac{-1}{\rho' \ln (b/a)}. \tag{2}$$

With the aid of the electric vector potential $\boldsymbol{F}$, where

$$\boldsymbol{F}(\boldsymbol{P}) = \frac{\epsilon_0}{4\pi} \int_{\substack{\text{frill} \\ \text{surface}}} \int \boldsymbol{M}'(\boldsymbol{P}') \frac{\exp(-jk|\boldsymbol{R}-\boldsymbol{R}|)}{|\boldsymbol{R}-\boldsymbol{R}'|} ds' \tag{3}$$

and the prime denotes source coordinates, one can determine the $\boldsymbol{E}$ and $\boldsymbol{H}$ fields by

$$\boldsymbol{E} = \frac{1}{j\omega\epsilon_0} \{\text{grad div} + k^2\}\boldsymbol{A} - \frac{1}{\epsilon_0} \text{curl } \boldsymbol{F} \tag{4}$$

$$\boldsymbol{H} = \frac{1}{j\omega\mu_0} \{\text{grad div} + k^2\}\boldsymbol{F} + \frac{1}{\mu_0} \text{curl } \boldsymbol{A}. \tag{5}$$

Since only magnetic currents are now present, $\boldsymbol{A} \equiv 0$.

For the near-zone-field values, numerical integration will first be used to obtain the electric vector potential,

and then numerical differentiation techniques are applied to calculate the fields. For larger observation distances (still near zone), closed-form expressions may be derived which not only simplify calculations but also validate the preceding numerical technique. The fields on the axis of the ring and in the far field are then given.

Theory

Numerical Technique for Near-Zone Fields

For the evaluation of $\boldsymbol{F}$ from (3), the incremental source area ds' on the frill is $\rho' d\rho' d\Phi'$. Dividing the frill into $d\rho'$ wide magnetic ring current, the contribution of each ring will be evaluated first, i.e., integration in Φ', before summing over all the rings. Because of the rotational symmetry of the problem (Φ independence), the observation point can further be located in the yz plane with no loss of generality (hence $\rho = y$ and $\boldsymbol{F}$ is Φ polarized). This results in the following expression for $\boldsymbol{F}$ from (2) and (3):

$$F_\Phi = -\frac{\epsilon_0}{2\pi \ln (b/a)} \int_a^b \int_0^\pi \cos \Phi' \frac{\exp(-jkR')}{R'} d\Phi' \, d\rho'. \tag{6}$$

The term $|\boldsymbol{R} - \boldsymbol{R}'|$ from (3), denoted now simply as R', can be seen from Fig. 2 to be

$$R' = [(z - z')^2 + \rho^2 + \rho'^2 - 2\rho\rho' \cos \Phi']^{1/2}. \tag{7}$$

Considering the ring in the xy plane (Fig. 3), each pair of incremental current element $d\Phi'$, symmetrically located at $\pm\Phi'$, has only a net $\hat{\Phi}$ contribution, thus resulting in the 2 cos Φ' factor with integration of Φ' from 0 to π.

Numerical integration may now be used to evaluate (6). Typically, integration in $d\rho'$ can be done very accurately by summing over merely five or less equally divided segments. If b/a now becomes large, then of course more segments may be needed. The integration in $d\Phi'$, on the other hand, can also be obtained directly, but the following subtraction of singularities simplifies the calculations. Suppose now the observation point is close to the source, i.e., $\rho \simeq \rho'$ in Fig. 2. Then $R' \to 0$ as $\Phi' \to 0$, thus yielding a singular integrand in (6). Removing this singular term results in

$$F_\Phi = \frac{-\epsilon_0}{2\pi \ln (b/a)} \int_a^b \left[\int_0^\pi \frac{d\Phi'}{R'} + \int_0^\pi \left(\cos \Phi' \frac{\exp(-jkR')}{R'} - \frac{1}{R'} \right) d\Phi' \right] d\rho' \tag{8}$$

where the second integral now has a well-behaved integrand. Furthermore, it may be shown that

$$\int_0^\pi \frac{d\Phi'}{R'} = \frac{2}{R_1} K\left(\frac{\pi}{2}, p^2\right) \tag{9}$$

where

$$R_1 = [(z - z')^2 + (\rho + \rho')^2]^{1/2} \tag{10}$$

$$p^2 = \frac{4\rho\rho'}{(z - z')^2 + (\rho + \rho')^2} \tag{11}$$

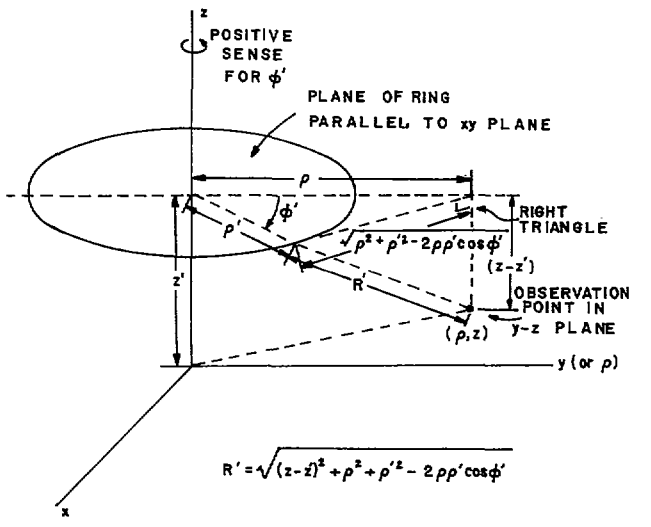

Fig. 2. Detailed geometry for source and observation coordinates for ring.

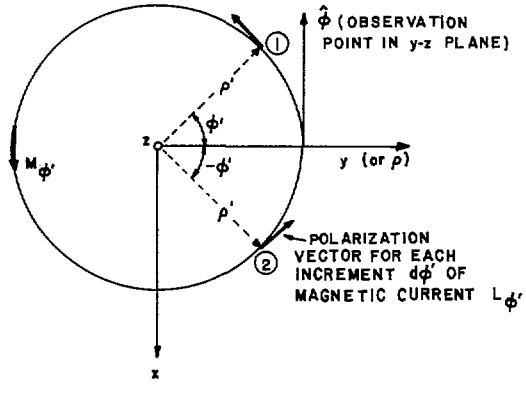

Fig. 3. Polarization vectors for source and observation coordinates.

and $K(\pi/2,p^2)$ is the complete elliptical integral of the first kind with a readily available polynomial approximation algorithm [10] for its computation. Equations (8) and (9) may now be used for the accurate numerical determination of F_Φ at any observation point not on the frill surface (even for $\rho < a$). The second integral in (8) may be evaluated by Simpson's rule and, typically, a division of only five segments from 0 to π for Φ' gives convergent results. (For $\rho < a$, up to 15 divisions may be needed).

To find the fields from the vector potential numerical differentiation is used. From (4) and (5), and for the cylindrical coordinate system, we obtain

$$E_z = -\frac{1}{\epsilon_0} \frac{1}{\rho} \frac{\partial}{\partial \rho} (\rho F_\Phi) \tag{12}$$

$$E_\rho = \frac{1}{\epsilon_0} \frac{\partial}{\partial z} (F_\Phi) \tag{13}$$

$$H_\Phi = -j\omega F_\Phi \tag{14}$$

where E_Φ, H_ρ, and H_z are identically zero. The partial derivatives may be evaluated numerically using Lagrange's three-point (equally spaced abscissas) formula [10],

which is

$$f_p' = f'(x_0 + ph) = \frac{1}{h}\left\{\left(p - \frac{1}{2}\right)f_{-1} - 2pf_0 + \left(p + \frac{1}{2}\right)f_1\right\} \tag{15}$$

where x_0 is the center point in the range $\pm ph$ (now either ρ or z) in which the derivative is needed and $f_{\pm 1}$ is the value of the function at $x = x_0 \pm h$. The corresponding four-point formula

$$f_p' = f'(x_0 + ph) = \frac{1}{h}\left\{-\frac{3p^2 - 6p + 2}{6}f_{-1} + \frac{3p^2 - 4p - 1}{2}f_0 - \frac{3p^2 - 2p - 2}{2}f_1 + \frac{3p^2 - 1}{6}f_2\right\} \tag{16}$$

is used both as an accuracy check and to calculate (13) when $z = z'$ (in the plane of the frill). Except at $z = z'$ or $\rho \equiv 0$, computations using (15) or (16) converged to better than 2 percent. Since F_Φ was found to be a rather well-behaved function, the usual numerical differentiation sensitivity to h, the differentiation interval [11], was not evident. Variations in h by orders of magnitude yielded negligible differences in field values. For convenience, h can be selected to be $b/100$.

Closed-Form Expressions for the Far Near Zone ($\rho \gg b$)

Closed-form expressions for $\boldsymbol{E}$ and $\boldsymbol{H}$ can now be derived in order to both simplify calculations when $\rho \gg b$ and to provide a further check on the accuracy of the preceding numerical technique. The usual far-field or Fresnel-zone approximations are not used here because $\lambda \gg \rho \gg b$, hence this may be thought of as a "far near-zone" form.

From (7), let

$$R_0 = [(z - z')^2 + \rho^2]^{1/2} \tag{17}$$

and after suitable series approximations on (6) one finds

$$F_\Phi(\rho,z) \simeq \frac{-\epsilon_0}{4 \ln (b/a)} k\rho \frac{\exp(-jkR_0)}{R_0^2}(b^2 - a^2) \cdot \left\{\frac{-j(b^2 + a^2)}{4R_0^2} + \frac{1}{2kR_0} + \frac{j}{2}\right\}. \tag{18}$$

From (12)-(14), the closed-form field expressions are then

$$\frac{E_\rho}{k} \simeq -\frac{(b^2 - a^2)}{8 \ln (b/a)} \rho \frac{(z - z')}{R_0} \frac{\exp(-jkR_0)}{R_0^2} \cdot \left\{k - \left(\frac{3}{k} + \frac{k(b^2 + a^2)}{2}\right)\frac{1}{R_0^2} + j\left[\frac{2(b^2 + a^2)}{R_0^3} - \frac{3}{R_0}\right]\right\} \tag{19}$$

$$\frac{E_z}{k} \simeq \frac{(b^2 - a^2)}{8 \ln (b/a)} \frac{\exp(-jkR_0)}{R_0^2}\left\{2\left(\frac{1}{kR_0} + j - \frac{j(b^2 + a^2)}{2R_0^2}\right) + \frac{\rho^2}{R_0}\left[\left(\frac{1}{kR_0} + j - \frac{j(b^2 + a^2)}{2R_0^2}\right)\left(-jk - \frac{2}{R_0}\right) + \left(\frac{-1}{kR_0^2} + j\frac{(b^2 + a^2)}{R_0^3}\right)\right]\right\} \tag{20}$$

$$\frac{H_\Phi}{k} \simeq \frac{j}{120\pi} \frac{(b^2 - a^2)}{8 \ln (b/a)} k \cdot \left[\rho \frac{\exp(-jkR_0)}{R_0^2}\left(\frac{1}{kR_0} + j - \frac{j(b^2 + a^2)}{2R_0^2}\right)\right]. \tag{21}$$

Axial Form ($\rho = 0$)

On the axis, at $\rho = 0$, the Φ symmetry of the problem dictates that $E_\rho(0,z) \equiv 0$. Equations (19)-(21), however, are no longer accurate when $\rho \to 0$. Consequently, a simple form for axial fields must be given. At $\rho = 0$, we have $R' = [(z - z')^2 + \rho'^2]^{1/2}$, hence

$$F_\Phi(0,z) = -\frac{\epsilon_0}{4\pi \ln (b/a)} \cdot \int_a^b \frac{\exp(-jkR')}{R'}\left[\int_0^{2\pi} \cos\Phi' \, d\Phi'\right] d\rho' \equiv 0. \tag{22}$$

Then

$$H_\Phi(0,z) \equiv 0. \tag{23}$$

From (12),

$$E_z(0,z) = -\frac{1}{\epsilon_0}\frac{F_\Phi}{\rho} - \frac{1}{\epsilon_0}\frac{\partial}{\partial\rho}F_\Phi = -\frac{2}{\epsilon_0}\frac{\partial F_\Phi}{\partial\rho}\bigg|_{\rho=0} \tag{24}$$

where l'Hospital's rule is used to account for the 0/0 term. Interchanging the order of integration and differentiation and carrying out the details, we find simply [2], [12]

$$E_z(0,z) = \frac{1}{\pi}\frac{1}{\ln (b/a)} \cdot \int_a^b \int_0^\pi \cos\Phi' \left[\frac{\partial}{\partial\rho}\frac{\exp(-jkR')}{R'}\right]_{\rho=0} d\Phi' \, d\rho' = \frac{1}{2 \ln (b/a)}\left\{\frac{\exp[-jk[(z - z')^2 + a^2]^{1/2}]}{[(z - z')^2 + a^2]^{1/2}} - \frac{\exp[-jk[(z - z')^2 + b^2]^{1/2}]}{[(z - z')^2 + b^2]^{1/2}}\right\}. \tag{25}$$

Equation (25) has been derived rigorously with no approximations, hence it may be regarded as a standard to check the accuracy of the numerical form. In summary, the near-zone fields of the magnetic frill source can be

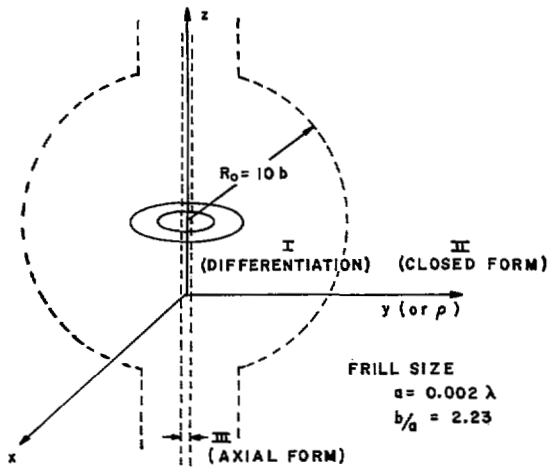

Fig. 4. Regions of applicability for various methods of computing near field of magnetic frill source.

TABLE I
COMPARISON OF AXIAL FIELDS E_z/k FOR A FRILL WITH DIMENSIONS ($a = 0.06\lambda$, $b = 0.065\lambda$)

$z(\lambda)$	Axial Form (25) (Exact)	Numerical Solution
0.01	$1.34083 \angle -1.03884°$	$1.33949 \angle -1.03873°$
0.02	$1.20423 \angle -1.15519°$	$1.20389 \angle -1.15584°$
0.03	$1.02382 \angle -1.356608°$	$1.02387 \angle -1.35584°$
0.04	$0.839214 \angle -1.64989°$	$0.839089 \angle -1.64991°$
0.06	$0.537892 \angle -2.55444°$	$0.537786 \angle -2.55534°$
0.10	$0.229912 \angle -5.83331°$	$0.229877 \angle -5.83356°$
0.20	$0.053865 \angle -22.5689°$	$0.053862 \angle -22.5712°$

calculated by a combination of the various methods just described. A discussion of their accuracies and convergences will be given in the results section. Their respective regions of applicability are illustrated in Fig. 4.

Far-Field Expressions

With suitable series approximations the far-zone potential and fields for even relatively large frills, i.e., $\lambda \simeq \rho' \ll R_0$, are given by

$$F_\Phi \simeq -\frac{\epsilon_0}{4}\frac{1}{\ln (b/a)} j \frac{\exp(-jkR_0)}{R_0}\frac{\pi(b^2-a^2)}{2} \cdot \left\{\frac{k\rho}{R_0} - \frac{1}{16}\left(\frac{k\rho}{R_0}\right)^3 (b^2+a^2)\right\} \quad (26)$$

$$E_\theta \simeq -\frac{\pi^2}{2}\frac{(b^2/\lambda^2 - a^2/\lambda^2)}{\ln (b/a)} \cdot \left\{\sin\theta - \frac{\pi^2}{4}\left(\frac{b^2}{\lambda^2}+\frac{a^2}{\lambda^2}\right)\sin^3\theta\right\}\frac{\exp(-jkR_0)}{R_0}. \quad (27)$$

Simple Magnetic Ring Sources ($b = a$)

In the limit as $b \to a$, the magnetic current then becomes $M_\Phi'(\rho') = \delta(\rho' = a)$. In this case the numerical method for near-field computations derived originally for the frill would apply with but a minor modification [12]. The axial form ($\rho = 0$) can be derived, in manner similar to the frill, with the result

$$E_z(0,z) = \frac{a^2}{2}\left[jk + \frac{1}{R'}\right]\frac{\exp(-jkR')}{R'^2},$$

with

$$R' = [(z-z')^2 + a^2]^{1/2}. \quad (28)$$

It should be noted that (28) is exact, whereas a similar expression in [13] assumes $a \gg \lambda$ (hence the absence of the $1/R'$ term). The far field for the simple ring can be integrated in closed-form with the resulting expression [6], [12]

$$E_\theta = -\frac{ka}{2} J_1(ka \sin\theta)\frac{\exp(-jkR_0)}{R_0} \quad (29)$$

where J_1 is the Bessel function of the first order.

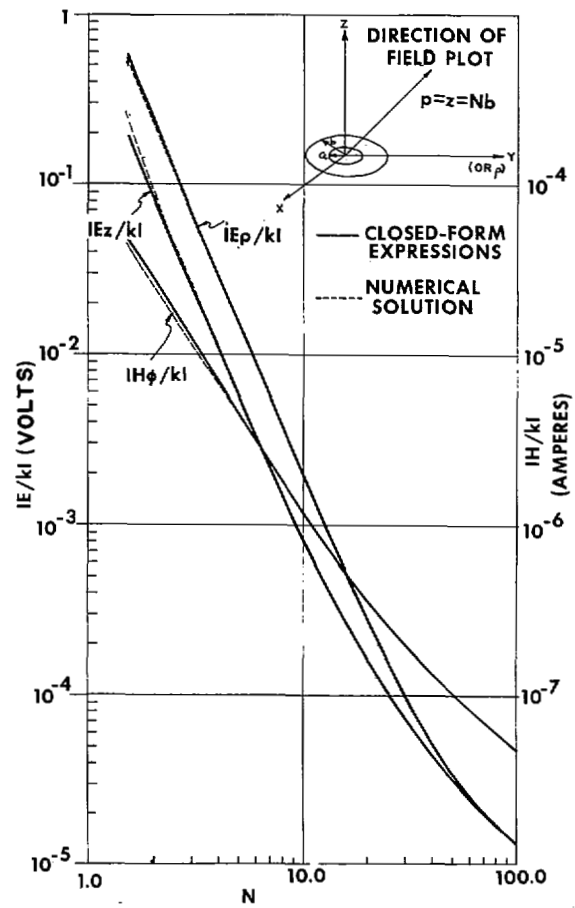

Fig. 5. Comparison of fields calculated by numerical solution with closed-form expression along 45° line in yz plane for frill with $a = 0.002\lambda$, $b = 0.005\lambda$.

Discussions and Results

In this presentation numerical techniques are used, and a simple and efficient method for calculating the vector potential was obtained because the singular part of its integral can be expressed as a known function (elliptical integral). The E and H fields are then conveniently evaluated by numerical differentiation methods. Consider now the complexity involved if the fields were to be calculated

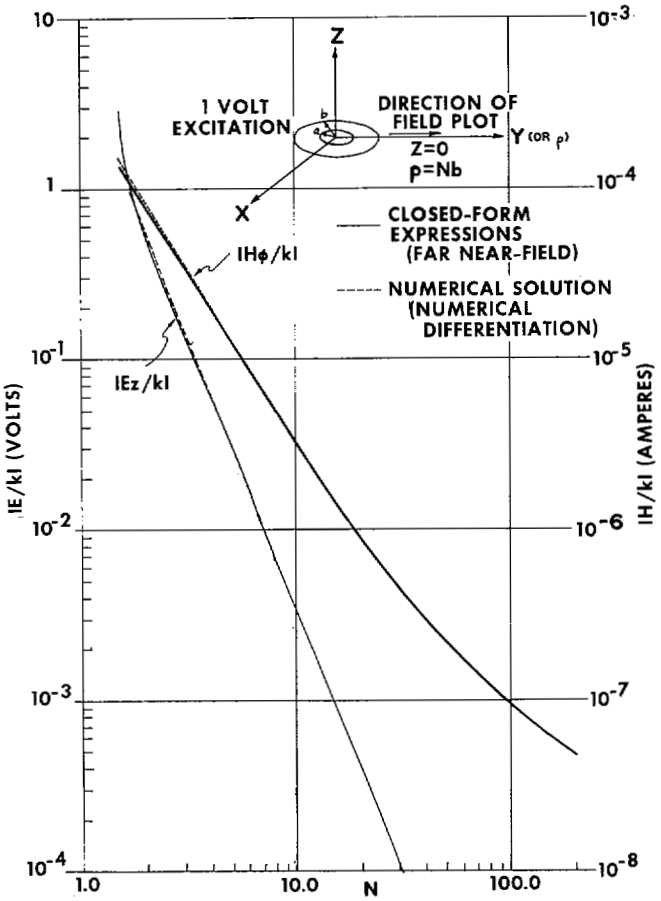

Fig. 6. Comparison of numerical solution to closed-form expression in plane of frill with $a = 0.002\lambda$, $b = 0.005\lambda$.

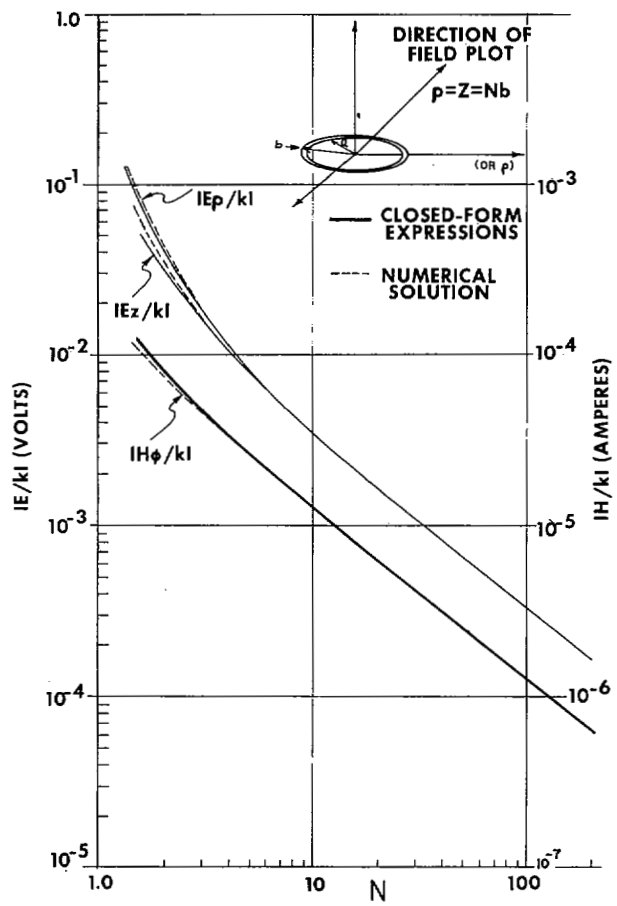

Fig. 7. Comparison of numerical solution to closed-form expressions along 45° line with $a = 0.06\lambda$, $b = 0.065\lambda$.

by more conventional methods. Interchanging the order of differentiation and integration, the near fields can be found from

$$E_\rho = \frac{1}{2\pi}\frac{1}{\ln\,(b/a)}\int_a^b\int_0^\pi \left(jk+\frac{1}{R'}\right)\frac{\exp\,(-jkR')}{R'^2} \cdot (z-z')\cos\Phi'\,d\phi'\,d\rho' \quad (30)$$

$$E_z = \frac{1}{2\pi}\frac{1}{\ln\,(b/a)}\int_a^b\int_0^\pi \cos\Phi'\frac{\exp\,(-jkR')}{R'} \cdot\left[\frac{1}{\rho}-\left(jk+\frac{1}{R'}\right)\frac{(\rho-\rho'\cos\Phi')}{R'}\right]d\Phi'\,d\rho' \quad (31)$$

$$H_\Phi = \frac{j\omega\epsilon_0}{2\pi}\frac{1}{\ln\,(b/a)}\int_a^b\int_0^\pi \cos\Phi'\frac{\exp\,(-jkR')}{R'}\,d\phi'\,d\rho'. \quad (32)$$

However, there now may occur singularities of the order $(1/R'^2)$ and $(1/R'^3)$ which would require significantly more numerical integration time and, furthermore, we will have three different integrands to contend with.

Since numerical differentiation is not a frequently used method, its accuracy needs to be carefully checked. Toward this end we compare the results from the numerical solution (7)–(16) with those from the axial form (25) and the far near-zone expressions (19)–(21) in their respective regions of validity. Table I compares E_z along the z axis as calculated from (25), which is exact, and the numerical solution using four-point differentiation. Close agreement is noted even for $z < a$. Figs. 5–7 give the comparison between the closed-form expressions in the far near zone and the numerical solution. In Fig. 5 the field plot is along a 45° line ($\rho = z = Nb$), while Fig. 6 plots the field in the plane of the frill for a small frill with dimensions $a = 0.002\lambda$, $b = 0.005\lambda$. Fig. 7 gives the results for a larger frill ($a = 0.06\lambda$, $b = 0.065\lambda$). As can be seen, the numerical solution converges quite closely to the closed-form expressions with increasing N (when (19)–(21) become valid). In fact, farther away from the frill, i.e., at $N \geq 100$, where numerical differentiation is perhaps least accurate, the agreement between the two methods was found to be better than four significant figures for all field components. From Figs. 5–7, the switching from the numerical solution to the closed-form expressions depicted in Fig. 4 can be empirically selected as $R_0 = 10b$.

As an additional check, the electric fields computed using numerical differentiation, (12) and (13), are compared to those using only numerical integration, (30) and (31). Tables II and III give the E_ρ and E_z along a 45°

TABLE II
COMPARISON OF E_ρ/k FOR A FRILL WITH DIMENSIONS ($a = 0.003\lambda$, $b = 0.005\lambda$) ALONG A 45° LINE

$\rho = z$ (λ)	Numerical Integration (30)	Numerical Differentiation (13)
0.0005	$0.5576263E + 0 + j0.7576563E\text{-}8$	$0.5574430E + 0 + j0.4139300E\text{-}5$
0.0015	$0.4047861E + 1 + j0.5202933E\text{-}7$	$0.4040245E + 1 - j0.1468615E\text{-}5$
0.0035	$0.4298512E + 1 + j0.4292932E\text{-}7$	$0.4299359E + 1 + j0.6686963E\text{-}6$
0.0055	$0.1683159E + 1 - j0.2954753E\text{-}7$	$0.1683143E + 1 - j0.3253601E\text{-}6$
0.0075	$0.7301296E + 0 - j0.1660948E\text{-}7$	$0.7302407E + 0 + j0.7756228E\text{-}7$
0.0095	$0.3711905E + 0 - j0.6506248E\text{-}8$	$0.3712679E + 0 - j0.1284663E\text{-}6$

TABLE III
COMPARISON OF E_z/k FOR A FRILL WITH DIMENSIONS ($a = 0.003\lambda$, $b = 0.005\lambda$) ALONG A 45° LINE

$\rho = z$ (λ)	Numerical Integration (31)	Numerical Differentiation (12)
0.0005	$0.2047232E + 2 - j0.1278110E\text{-}3$	$0.2046579E + 2 - j0.1119673E\text{-}3$
0.0015	$0.1688541E + 2 - j0.1159331E\text{-}3$	$0.1688470E + 2 - j0.1044982E\text{-}3$
0.0035	$0.4387288E + 1 - j0.1070034E\text{-}3$	$0.4387884E + 1 - j0.1037690E\text{-}3$
0.0055	$0.1019517E + 1 - j0.1050501E\text{-}3$	$0.1019675E + 1 - j0.1042650E\text{-}3$
0.0075	$0.3493413E + 0 - j0.1045860E\text{-}3$	$0.3491055E + 0 - j0.1038956E\text{-}3$
0.0095	$0.1576679E + 0 - j0.1053756E\text{-}3$	$0.1576202E + 0 - j0.1035746E\text{-}3$

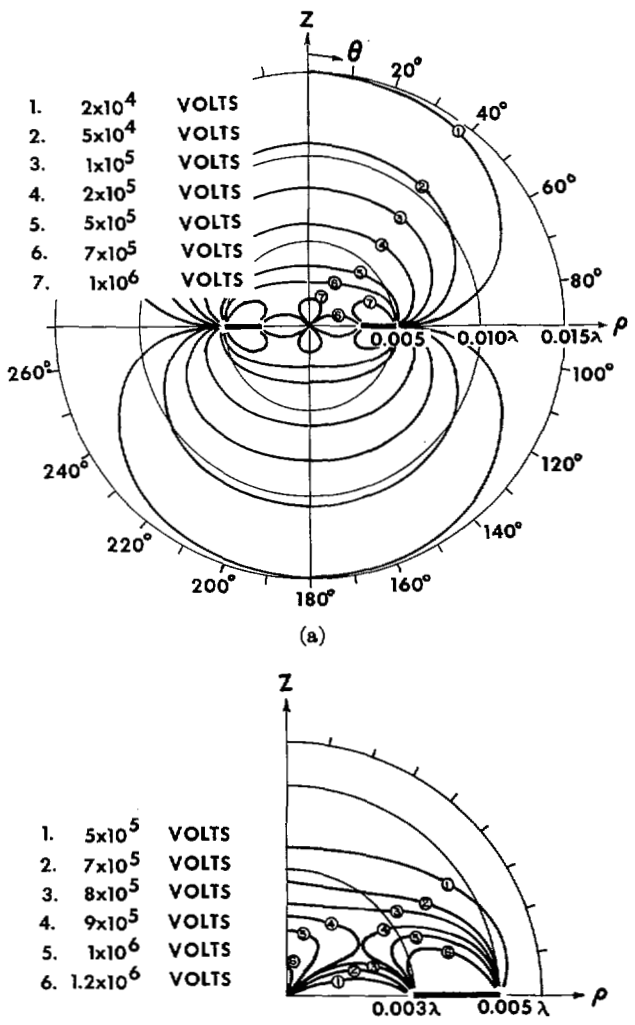

Fig. 8. (a) Near-field constant $|E_r/k|$ contours for small frill with $a = 0.003\lambda$, $b = 0.005\lambda$. (b) Expanded center.

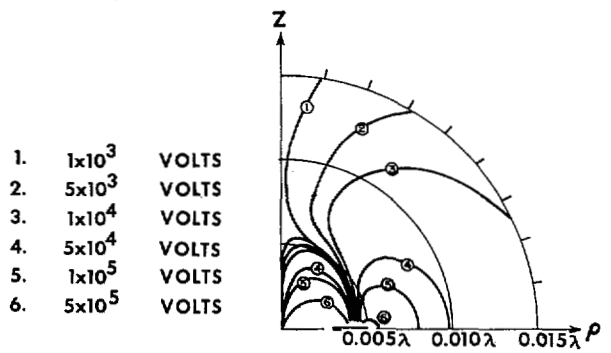

Fig. 9. Near-field constant E_θ/k contours for $a = 0.003\lambda$, $b = 0.005\lambda$.

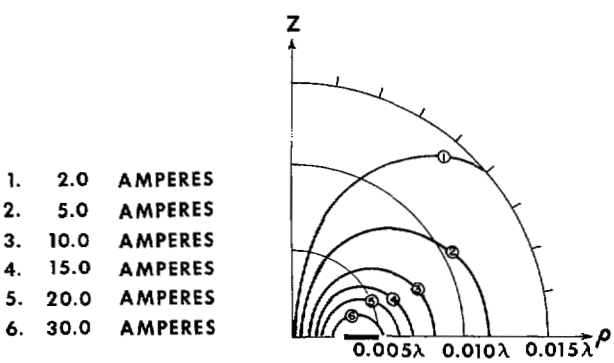

Fig. 10. Near-field constant $|H_\phi/k|$ contours for $a = 0.003\lambda$, $b = 0.005\lambda$.

line for a frill with $a = 0.003\lambda$ and $b = 0.005\lambda$. For these cases, because the observation distance is actually smaller than the frill radius, a larger number of integration intervals are required for convergence. As can be seen, the agreement is excellent. It is also worth noting that (12)

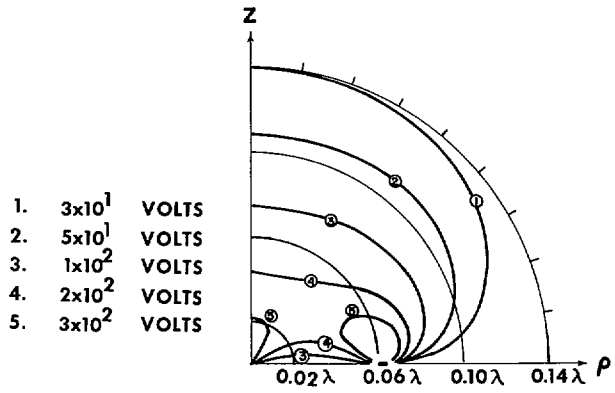

Fig. 11. Near-field constant $|E_r/k|$ contours for larger frill with $a = 0.06\lambda$, $b = 0.0625\lambda$.

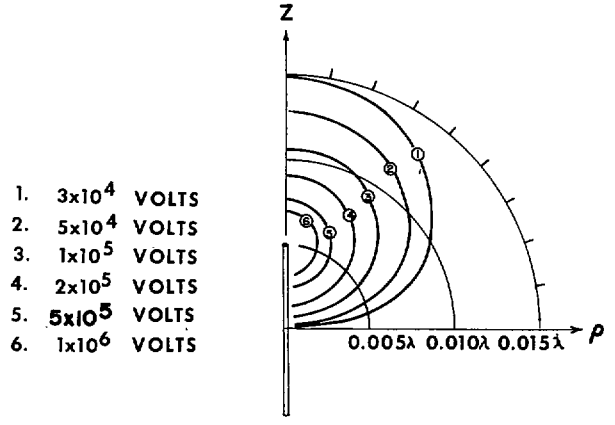

Fig. 12. Near-field constant $|E_r/k|$ contours for short electric dipole with constant current distribution and length = 0.01λ.

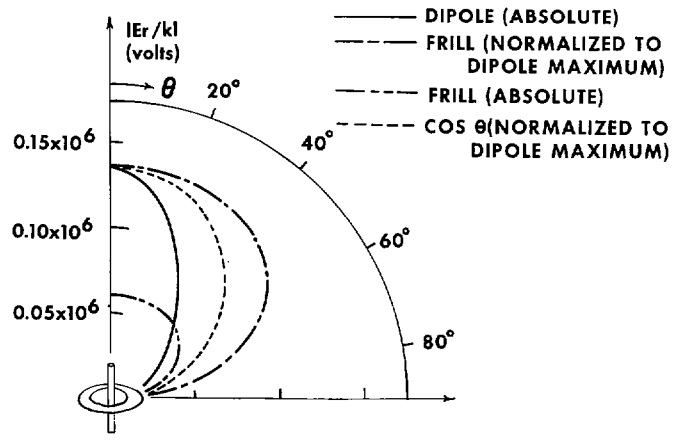

Fig. 13. Comparison of electric dipole and magnetic frill current near-zone E_r patterns on constant radius circle ($R = 2b = 0.01\lambda$) for frill with $a = 0.003\lambda$, $b = 0.005\lambda$, and dipole length = 0.010λ.

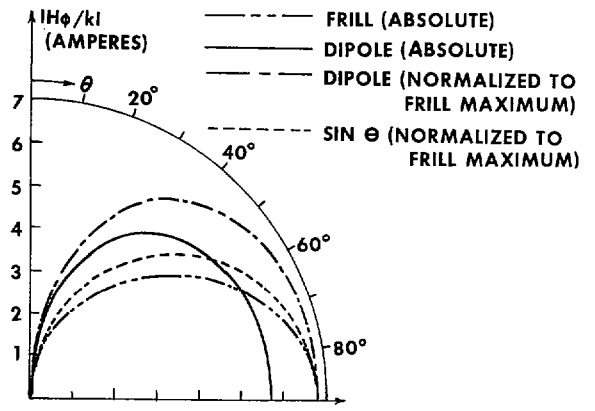

Fig. 14. Comparison of electric dipole and magnetic frill source H_ϕ near-zone patterns ($R = 2b = 0.01\lambda$).

and (13) requires only one fourth the computer time required by (30) and (31).

From the preceding agreement among the various methods in their mutual regions of validity, it may be concluded that the numerical procedures employed can indeed efficiently give very accurate near-field information. Typical computation time is 15 ms on the IBM 7094 computer. Furthermore, the ease with which numerical differentiation may be used when functions are well behaved indicates that its use should be considered for other electromagnetic field problems.

Near-field contour maps in the yz plane are now presented for two different frill sizes. E_r, E_θ, and H_Φ (the spherical components) are given in Figs. 8–10 for a small frill with $a = 0.003\lambda$, $b = 0.005\lambda$. The magnitudes are normalized so that the total far-field radiated power from the source is 1 W. Fig. 11 similarly gives the E_r contours for a larger frill, $a = 0.06\lambda$, $b = 0.0625\lambda$.

It is interesting to note that the well-known duality between infinitesimal electric dipoles and magnetic loops does not hold in the near field for sources that are merely small. Fig. 12 depicts the E_r contours for an electric line source with a constant current and having the same overall physical dimensions as the frill in Fig. 8. 1-W total radiated power normalization is used also with E_r computed by summing over 100 incremental dipoles. For a source even as small as 0.01λ, as can be seen by comparing Figs. 8 and 12, the near fields of magnetic loops and electric dipoles are different. This difference is further illustrated in the near-zone patterns for the two sources (Figs. 13 and 14), where E_r and H_Φ are plotted as a function of θ along a constant radius circle at $r = 2b$. If the sources were infinitesimally small, then their patterns would both coincide with the respective sine and cosine patterns shown [14]. Hence duality for these small sources should only be used at large observation distances.

Even though this paper considered contributions only from the TEM mode in the coaxial aperture, the numerical technique presented is not necessarily restricted to this case. It should be possible to include the fields from the higher order mode aperture currents by analogous techniques once these currents are determined. For large structures these contributions may be significant and the method described in [8], [9] can be used for the solution of these currents.

Applications

While the near-field variation for the basic magnetic ring source presents an interesting problem in its own right, it is also quite useful for practical applications.

Accurate near fields would be desirable for studies of high-power breakdown phenomena in ring slot antennas or mutual coupling effects among elements of an array of such slots. In addition to these direct applications, extensions may be made using the magnetic frill source as a basic building block to analyze complex antenna geometries which are fed coaxially. In the discussions to follow several examples are briefly described which used the frill either as a primary radiator or as equivalent sources.

Employing the magnetic frill as the driving source, the impedance of the Yagi–Uda antenna has been successfully analyzed [15], [16]. Using a Fourier series expansion for the currents on the wires with the coefficients determined by point-matching techniques, the near fields of the frill calculated by the method in this paper then constituted the input, or the right-hand side, of the system of simultaneous equations. Excellent agreement was reported between calculated and measured results for a four-element array over a wide frequency range. Using similar techniques, the problems of a coaxially fed circular loop over a ground plane and a ring slot antenna at the base of a conducting cone were also successfully treated [16].

Using the magnetic frills as equivalent sources, a synthesis method was carried out for the solution of coaxially fed dipole antennas symmetrically mounted on a conducting sphere or cylinder [12], [17]. The basic idea is that an array of axially distributed magnetic frills can be found which will approximately satisfy boundary conditions on the spherical (or cylindrical) surface. Each frill, of course, excites some current distribution on the wire antenna with the superposition of the near fields from all these sources constituting the total solution. Provided boundary conditions are met, the equivalent source solution will then generate the same exterior fields and currents as the original structure with its solid conducting sphere (or cylinder). For these problems also, close correlation was obtained between measured and calculated input admittances, radiation patterns, and resonance behaviors.

Conclusion

An analytically simple method has been obtained for the calculation of near-zone as well as far-zone fields from an annular ring of magnetic current. For the near fields, an efficient method was developed which uses numerical integration and differentiation. Closed-form expressions have also been derived for the far near-zone and along the axis of symmetry. From the close agreement among the various formulations in their mutual regions of validity, a direct check on their accuracy was established. The utility of this solution was further demonstrated through its application in several practical antenna problems. Because of its efficiency, accuracy, and utility, it is believed that the techniques and results of this solution may be useful for many other electromagnetic problems.

Acknowledgment

The author wishes to express his gratitude to Dr. D. V. Otto, who provided much of the guidance in the early phase of this study.

References

[1] G. E. Albert and J. L. Synge, "The general problem of antenna radiation and the fundamental integral equation, with application to an antenna of revolution, pt. I," *Quart. Appl. Math.*, vol. 6, no. 1, pp. 117–131, 1948.
[2] D. V. Otto, "Cylindrical antenna theory," Ph.D. dissertation, Univ. Aukland, Aukland, New Zealand, 1967.
[3] ——, "The admittance of cylindrical antennas driven from a coaxial line," *Radio Sci.* (New Series), vol. 2, no. 9, pp. 1031–1042, 1967.
[4] ——, "Fourier transform method in cylindrical antenna theory," *Radio Sci.* (New Series), vol. 3, no. 11, pp. 1050–1057, 1968.
[5] N. Foo, "Radiation fields of an annular source of radially directed currents," *IEEE Trans. Antennas Propagat.* (Commun.), vol. AP-17, p. 658, Sept. 1969.
[6] E. A. Wolff, *Antenna Analysis*. New York: Wiley, 1966, pp. 166–169.
[7] R. F. Harrington, *Time Harmonic Electromagnetic Fields*. New York: McGraw-Hill, 1961, pp. 93, 110–113.
[8] D. C. Chang, "Input admittance and complete near-field distribution of an annular aperture antenna driven by a coaxial line," *IEEE Trans. Antennas Propagat.*, vol. AP-18, pp. 610–616, Sept. 1970.
[9] C. W. Harrison, Jr., and D. C. Chang, "Theory of the annular slot antenna based on duality," *IEEE Trans. Electromagn. Compat.*, vol. EMC-13, pp. 8–14, Feb. 1971.
[10] M. Abramowitz and I. T. Stegun, Ed., *Handbook of Mathematical Functions* (Applied Mathematics Series 55). Washington, D. C.: NBS, 1964, pp. 589–591, 883–885.
[11] A. Ralston, *A First Course in Numerical Analysis*. New York: McGraw-Hill, 1965, pp. 79–83.
[12] L. L. Tsai, "Analysis and measurement of a dipole antenna mounted symmetrically on a conducting sphere or cylinder, Ph.D. dissertation, Dep. Elec. Eng., Ohio State Univ., Columbus; also published as ElectroScience Laboratory, Ohio State Univ., Rep. 2648-3 under M.I.T. Lincoln Lab. Contract AF 19 (628)-5167, 1970.
[13] H. E. Green, "Impedance of a monopole on the base of a large cone," *IEEE Trans. Antennas Propagat.*, vol. AP-17, pp. 703–706, Nov. 1969.
[14] J. D. Kraus, *Antennas*. New York: McGraw-Hill, 1950, pp. 127–135.
[15] G. A. Thiele, "Impedance analysis of Yagi–Uda type antennas," in *Dig. 1969 URSI Fall Meeting*.
[16] ——, "Wire antennas," in *Computer Techniques for Electromagnetics and Antennas* (a short course at the University of Illinois), R. Mittra, Ed., 1970, ch. 2.
[17] L. L. Tsai, "Dipole antennas mounted on a conducting sphere or cylinder," in *1970 IEEE G-AP Symp. Dig.*